Featured in Physics

Transient Supersolid Properties in an Array of Dipolar Quantum Droplets

Fabian Böttcher, Jan-Niklas Schmidt, Matthias Wenzel, Jens Hertkorn, Mingyang Guo, Tim Langen, and Tilman Pfau*

5. Physikalisches Institut and Center for Integrated Quantum Science and Technology, Universität Stuttgart, Pfaffenwaldring 57, 70569 Stuttgart, Germany

(Received 23 January 2019; published 22 March 2019; corrected 25 April 2019)

We study theoretically and experimentally the emergence of supersolid properties in a dipolar Bose-Einstein condensate. The theory reveals a ground state phase diagram with three distinct regimes—a regular Bose-Einstein condensate and incoherent and coherent arrays of quantum droplets. The coherent droplets are connected by a background condensate, which leads—in addition to the periodic density modulation—to a robust phase coherence throughout the whole system. We further theoretically demonstrate that we are able to dynamically approach the ground state in our experiment and that its lifetime is limited only by three-body losses. Experimentally we probe and confirm the signatures of the phase diagram by observing the *in situ* density modulation as well as the phase coherence using matter wave interference.

DOI: 10.1103/PhysRevX.9.011051

Subject Areas: Atomic and Molecular Physics, Condensed Matter Physics, Quantum Physics

Whether a material is solid, liquid, or gaseous in classical physics depends on the strength of the interactions with respect to the motional energy of the particles. In analogy to this behavior the interplay between quantum fluctuations and interparticle interactions also leads to new phases of matter in quantum mechanics. One example of such quantum phases is the supersolid [1–6] featuring the periodic density modulation of a solid together with the dissipationless flow of a superfluid. While these properties are normally thought of as mutually exclusive, it was shown that they can actually coexist [2]. More formally speaking, a supersolid features both on- and off-diagonal long-range order in its density matrix [1]. Originally, supersolidity was mainly discussed in the context of ^{4}He, for which it remains elusive in the experiments [7]. The concept of supersolidity has since been generalized to other superfluid systems and supersolid properties have been observed in ultracold atomic systems for spin-orbit-coupled Bose-Einstein condensates (BECs) [8] as well as BECs symmetrically coupled to two crossed optical cavities [9,10]. In these systems the periodicity of the modulation is induced by the underlying periodic optical potentials. In contrast, there are physical systems where the self-organized structure formation is induced by the intrinsic interactions, and therefore phonon modes of the periodic modulation are allowed like in classical solids.

One promising system of this type is dipolar quantum gases [11,12], featuring both short-range contact interactions as well as long-range dipole-dipole interactions. These dipolar systems feature a rotonic dispersion relation similar to ^{4}He [13] which, in addition, is fully tunable by changing the contact interaction strength as well as the external confinement along the dipoles. This dispersion relation has been studied experimentally [14,15] and has led to the discovery of 2D arrays of quantum droplets [16–18]. However, it was shown that the 2D arrays in these early experiments were incoherent, excited states of the system. For the considered geometries the ground state was always a single droplet [19–22]. In contrast to this, in Ref. [23] we pointed out that the ground state in strongly confined 2D geometries is made up of droplet arrays, but we experimentally observed that these arrays rapidly lose their relative coherence during their dynamical formation process. So while each droplet is coherent by itself, there is no global phase coherence between different droplets. In this work we always refer to this global coherence of the system. Furthermore, increasing the overlap of the droplet wave functions through an increase of the remaining weakly confining trapping direction was proposed as a way to establish more robust phase coherence in experiments.

A recent theoretical study [24] examined a similar elongated trapping configuration with periodic boundaries along one axis perpendicular to the magnetic field. In this work it was shown that close to the softening of the roton

*t.pfau@physik.uni-stuttgart.de

mode droplets form, which are immersed in the dilute superfluid background of a BEC. This special case of coherent droplets forms only in a very narrow range of interaction strengths, while for smaller contact interaction strengths the background vanishes, leading to isolated droplets. The coherent droplets were shown to exhibit two distinct excitation modes, a phonon and a phase mode, which are hallmarks of supersolidity.

At the same time it was observed experimentally that phase-coherent droplets can exist for a narrow range of contact interaction strengths [25]. However, in this experiment only the phase information after time-of-flight expansion was accessible [26] and a detailed theoretical explanation of the observations is still lacking.

Here we present a comprehensive study of the supersolid properties of a trapped dipolar gas. First, we show theoretically that within the framework of the extended Gross-Pitaevskii equation (eGPE) a phase-coherent and density-modulated state can be reached dynamically for our elongated trap geometry. This state is found to be very close to the ground state of the system. Second, we experimentally realize such a state and observe its properties, both *in situ* and in time of flight. With these two complementary observation techniques we map out the signatures of the theoretical phase diagram that clearly reveals both a coherent and an incoherent density-modulated regime.

We start by looking at the theoretical ground state of the dipolar system within the framework of the eGPE. To this end, we numerically solve the eGPE using imaginary time propagation [23] to calculate the ground states. These simulations are performed for $(2\text{–}5) \times 10^4$ ^{162}Dy atoms in a harmonic potential with trapping frequencies $\omega = 2\pi(18.5, 53, 81)$ Hz similar to Ref. [25]. Depending on the contact interaction strength, this yields three distinct regimes, which are summarized on the right-hand side of Fig. 1(a) for an atom number of 3.5×10^4. While for high scattering lengths of $a_s \geq 95a_0$ the ground state is a regular BEC, at low scattering lengths $a_s \lesssim 90a_0$ we recover the thoroughly studied regime of isolated droplets [16,17,23,27]. The most interesting regime, e.g., for $a_s = 94a_0$, is found in between these two limits and consists of droplets that are immersed in a residual BEC background. This background acts as a link between the droplets and therefore establishes phase coherence.

With these observations in mind we quantify the transition in terms of the density link between the individual droplets, in particular between the central droplet and its nearest neighbors. To do this we analyze cuts through the center of the simulated densities $n = |\psi|^2$ and calculate the ratio between the first minimum and the central maximum. This simple measure characterizes the density overlap between neighboring droplets and is shown in Fig. 1(b). For a BEC there exists no density modulation and therefore we set this ratio to 100%. As soon as the density modulation emerges below $a_s \approx 94.5a_0$, this ratio is well

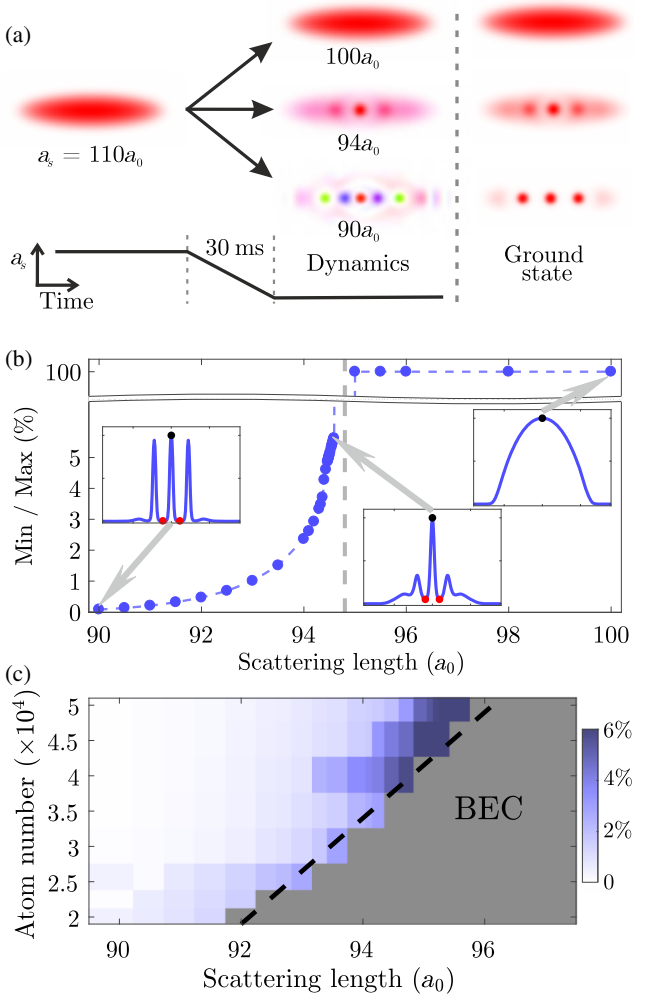

FIG. 1. Phase transition from BEC to immersed droplets to isolated droplets. (a) Schematic of the experimental sequence and corresponding ground states. We start from a BEC and then change the scattering length to its final value, where we observe three different regimes: at high scattering lengths a BEC, at low scattering lengths isolated droplets, and in between droplets immersed in a superfluid background. We compare the dynamical simulations to the corresponding ground states. The pictures show the phase in color scale weighted by the density distribution. (b) To quantify the transition we calculate the ratio of the first minimum compared to the center peak height of the ground state containing 3.5×10^4 atoms. (c) Ground state phase diagram of this calculated ratio for different atom numbers and scattering lengths. Note that with higher atom number, the number of droplets, and, as a consequence, also their overlap increases. The dashed black line is a guide to the eye.

defined and shows a distinct jump followed by a steady decrease for lower scattering lengths. Interpreting the overlap as an order parameter, this discontinuity is an indication of a first-order phase transition, further evidenced by the observation of hysteresis in our numerical simulations [28] and by the experimental signatures in Ref. [25]. Moreover, this behavior is reminiscent of the

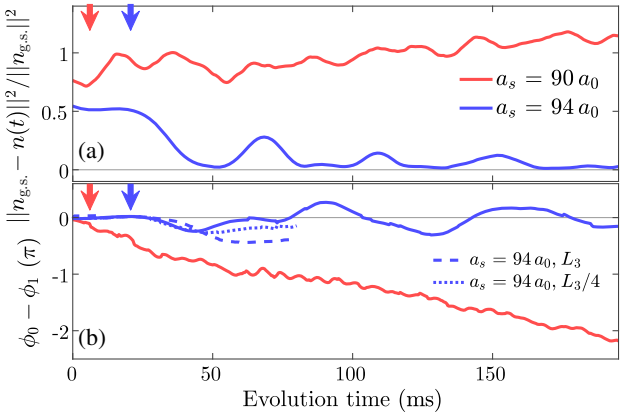

FIG. 2. Overlap of the calculated dynamical state with the ground state. (a) Time evolution of the density difference $\|n_{\mathrm{g.s.}} - n(t)\|^2/\|n_{\mathrm{g.s.}}\|^2$, where $n(t)$ is the dynamical density, $n_{\mathrm{g.s.}}$ is the ground state density, and $\|\cdots\|$ is the Euclidean norm. We observe little density overlap for the isolated droplets (red) and (except for a residual breathing mode) high density overlap for the coherent droplet state (blue). (b) Time evolution of the phase difference $\phi_0 - \phi_1$ between the central droplet and its nearest neighbor for the dynamical simulation. For the coherent droplet the phase difference caused during the formation process is rapidly compensated leading to a vanishing phase difference between the two neighboring droplets. On the other hand, the phase difference of isolated droplets increases almost linearly after the formation, which is due to their difference in chemical potential. Including three-body losses we see a constant (experimentally measured L_3, dashed line) or slowly decreasing ($L_3/4$, dotted line) phase difference during the lifetime of the droplets. The arrows indicate the respective formation time of the droplets for the two scattering lengths.

decrease of the superfluid fraction across the supersolid phase transition that was observed in previous works [24,29]. However, note that while the ratio shown in Fig. 1(b) is a measure of the overlap of the droplets, it does not directly correspond to the actual superfluid fraction. The superfluid fraction of the system was shown to notably exceed the values of this overlap ratio [24].

We extend this study to different atom numbers and show it as a phase diagram in Fig. 1(c). We observe a clear phase boundary where the density-modulated state becomes lower in energy than a regular BEC. This phase boundary shifts to higher scattering length with increasing atom number. While overall being located close to the roton instability, our observed scaling for the simulated ground states appears different from the approximate roton scaling for a trapped gas reported in Ref. [25], in particular at higher interaction strengths.

To study how one can dynamically establish a phase-coherent state in an experiment, we perform time-dependent simulations starting from the BEC ground state at $a_s = 110a_0$ and then linearly ramp the scattering length to its final value within 30 ms. A snapshot of the system after some evolution time is shown schematically in Fig. 1(a), where the dynamically reached states are compared to the calculated ground states. This comparison shows that for $a_s = 94a_0$, the dynamically calculated wave function is phase coherent and very close to the calculated ground state. In contrast to this for $a_s = 90a_0$, the phase of the individual droplets is different and also their number does not match the ground state prediction [23,28]. Using shorter ramp times in the dynamical simulations, we produce states with a different number of droplets also for $a_s = 94a_0$. Only for ramp times $\gtrsim 20$ ms we produce states that are close to the ground state of the system.

For a more quantitative comparison, we compare the overlap of the dynamically simulated wave function in real time with the ground state we get from the imaginary time evolution. We observe that incoherent droplets form soon after the end of the interaction ramp, while coherent droplets emerge slowly over several tens of milliseconds. This longer formation time for the coherent state is in agreement with a lower energy difference between this state and the initial BEC. In Fig. 2(a), we show the difference of the densities in the dynamical case $n(t)$ and the ground state $n_{\mathrm{g.s.}}$, and Fig. 2(b) depicts the evolution of the phase difference between the central droplet and its nearest neighbor, which is an indicator for their phase coherence. In the density difference one can see that for the case of isolated droplets the difference is significant and actually increases with time, while for the coherent droplets the difference approaches zero after the time required for the droplets to form. The oscillations visible in the density difference after the formation correspond to a breathing mode along the droplet array. In the phase difference we observe that for the isolated droplets the phase difference increases linearly after the formation. We attribute this to the different chemical potentials of the two droplets. In contrast to this, in the coherent regime we observe that the phase difference remains significantly smaller with very little variation over time. Our simulations thus reveal the existence of a state that is both density modulated and phase coherent and can be reached dynamically by an interaction ramp into a narrow range of interaction strengths. Given the superfluid fraction and excitation spectrum that were calculated in Ref. [24], we conclude that this state can be identified as a dipolar supersolid.

As a next step we include realistic three-body losses in the simulations with our experimentally measured loss coefficient $L_3 = 1.5 \times 10^{-40}$ m^6/s for $a_s = 94a_0$ [30], as well as for reference with a lower loss rate of $L_3/4$. When loss is included a comparison of the densities is challenging because the ground state continuously changes with atom number. Therefore, we restrict ourselves to the phase coherence shown in Fig. 2(b) and again observe only a small phase difference starting to form during the droplet formation process. However, this phase difference is rapidly stabilized and subsequently slowly decreases throughout the remaining lifetime of the state. An alternative way of characterizing the difference of the two wave functions is the

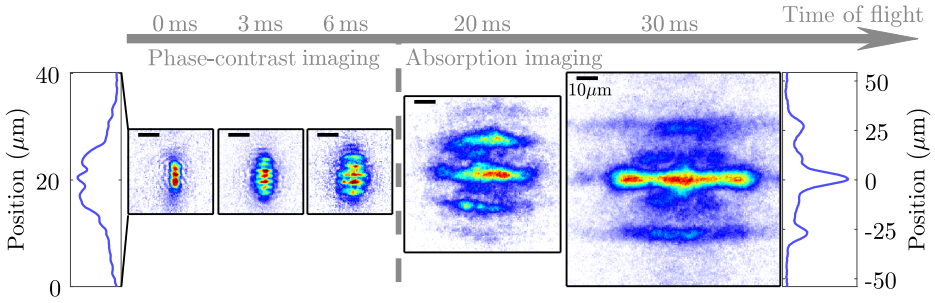

FIG. 3. Evolution from *in situ* density distribution to time-of-flight interference. On the left-hand side, we show an exemplary *in situ* image together with the integrated density distribution for the phase-coherent droplet regime, revealing a clear density modulation. Towards the right-hand side, we show the expansion dynamics for different times of flight, which exhibits the characteristic increase of the fringe spacing of expanding matter waves. On the very right, we show the interference pattern after 30 ms time of flight together with the corresponding integrated momentum distribution. In these interference patterns a clear substructure at half the principle fringe spacing can be seen. While the principle interference peaks yield information about the nearest-neighbor coherence, the additional peaks correspond to next-nearest-neighbor coherence. The individual images shown result from independent experimental realizations.

fidelity, defined as $\mathcal{F} = |\langle \Psi_{\mathrm{g.s.}} | \Psi(t) \rangle|^2$. Using this we get a numerical value of $\mathcal{F} \approx 90\%$ after our experimental equilibration time of 15 ms. This shows that we expect to dynamically create a state with transient supersolid properties very close to the actual ground state even in the presence of three-body losses.

In order to investigate the formation of a phase-coherent droplet state experimentally, we prepare a quasipure dipolar BEC with approximately 4.5×10^4 ^{162}Dy atoms at a temperature below 20 nK in a tubular trap with trap frequencies $\omega = 2\pi[19(1), 53(1), 87(1)]$ Hz and $\mathbf{B} \| \hat{z}$, similar to Ref. [25]. We compensate the gravitational force on the atoms by ramping up a magnetic field gradient, allowing for long times of flight to probe the system. Subsequently we change the scattering length from $\sim 140 a_0$ to $\sim 110 a_0$ by ramping the magnetic field in 80 ms closer to a double Feshbach resonances of ^{162}Dy located around 5.1 G [30,31]. In order to reach the droplet regime we subsequently ramp the magnetic field again linearly within 30 ms to the final scattering length in the range between $89 a_0$ and $98 a_0$ [32]. We then hold the atoms for 15 ms at this field in order to equilibrate. Finally, we probe the resulting state either *in situ* using far-detuned phase-contrast imaging or after time of flight using absorption imaging. As we are in or close to a regime where droplets are self-bound, we boost the time-of-flight expansion velocity by ramping up the scattering length to $\sim 140 a_0$ within 100 μs just before the release of the atoms from the trapping potential. This has the additional advantage that density rapidly decreases, minimizing interaction effects in the expansion. Moreover, it acts as a zoom greatly increasing the extent of the interference patterns, and thus, giving access to subtle features beyond simple nearest-neighbor phase coherence. As exemplified in Fig. 3, our experiment thereby reveals both the *in situ* density modulation as well as the interference pattern of multiple matter waves emerging after time of flight.

First, we analyze in more detail how the *in situ* density distribution changes for different atom numbers and final scattering lengths. Above a certain atom number threshold we observe the appearance of multiple droplets aligning along the weak axis of the trap. Experimentally this density modulation takes about 5–10 ms to develop. We attribute this faster formation time compared to the numerical simulations to fluctuations due to residual excitations and finite temperature, which can seed the underlying instabilities driving the phase transition. Because of our finite imaging resolution of 1 μm, the smaller size of the droplets, and the imaging aberrations arising thereupon, we cannot reliably extract the number of droplets or the overlap between droplets and the background BEC directly from our images. This resolution-limited imaging also leads to a larger uncertainty in the extracted atom number compared to the data obtained in time of flight. As in our previous work [16], we therefore use the absolute value of the Fourier transform of the integrated *in situ* density to identify images with a density modulation. To this end, we compare the spectral weight of finite momentum contributions to the weight of the central peak in momentum space [28]. This ratio is plotted as a function of scattering length and atom number in Fig. 5(a). Typically, every coordinate is an average of a few experimental runs with 80 realizations in total for every scattering length, and the different atom numbers have been realized by binning our experimental data. We observe that a density modulation appears above a certain atom number threshold and compare this to the boundary from the theoretical phase diagram. With this we can clearly map out a region showing a density-modulated state in the experiment. For small scattering lengths and high atom number, we see the modulation amplitude decreasing again, which is caused by a washing out of the mean distribution due to fluctuations in the number of droplets and therefore also their spatial separation.

Next, we study the phase coherence of the realized droplet states via interference after 30 ms time of flight. For our parameters we typically realize an array of several droplets. In contrast to the well-known interference of

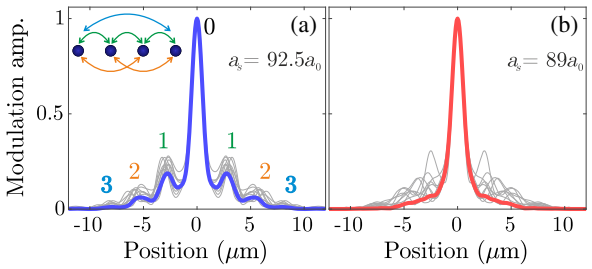

FIG. 4. Evaluation of the coherence between neighboring droplets. Absolute value of the Fourier transform of the integrated interference patterns after 30 ms time of flight, showing signs of the multiple frequencies of the interference due to nearest-neighbor, next-nearest-neighbor, and even higher-order coherence. This is schematically shown in the inset of (a). The gray lines correspond to single-shot realizations and the blue lines to the mean of all available realizations for a given atom number for $a_s = 92.5a_0$ [(a), blue] and $a_s = 89a_0$ [(b), red]. In the latter case, the position of the side peaks changes randomly (b), while in the coherent droplet regime (a), the side peaks appear at the same position in every realization and show very little variance in their amplitude. This provides clear evidence for the phase coherence between the droplets (a), with the variance of the peak height of the first side peak corresponding to nearest-neighbor coherence, the second peak corresponding to next-nearest-neighbor coherence, and the third to next-next-nearest-neighbor coherence. The shown exemplary Fourier transforms correspond to the red points in Figs. 5(b) and 5(c).

two BECs [33], our situation thus leads to a more complex interference pattern with multiple frequencies [28,34]. For the evaluation of our data we therefore again turn to the absolute value of the Fourier transform of the integrated image after time of flight. Note that this Fourier transform of the time-of-flight density, rather than the wave function, does not yield again the initial *in situ* wave function but rather provides information about the individual frequency components of the interference pattern. Examples of this for scattering lengths of $a_s = 92.5a_0$ and $a_s = 89a_0$ are shown in Figs. 4(a) and 4(b), respectively. The gray lines are single-shot realizations, while the blue and red lines show the mean of all available realizations for a given atom number and scattering length, with more than 300 realizations for every scattering length in total.

We observe a clear difference between the two scattering lengths, caused by two distinct effects. The data for $a_s = 92.5a_0$ can be identified with coherent droplets and show stable side peaks at the same position in every realization. The data for $a_s = 89a_0$ correspond to incoherent droplets and show strong fluctuations from realization to realization. The change in the side peak positions for the incoherent droplets is caused by a varying number of droplets and, therefore, a different initial separation from shot to shot, while the stable position of the side peaks for the coherent droplets means that the initial state is very reproducible. In particular, as in the usual double-slit interference, the height of the Fourier peaks is a measure of the interference contrast and their shot-to-shot variation thus encodes the phase coherence of the system. In our case, the individual Fourier peaks characterize nearest-neighbor, next-nearest-neighbor, and even higher-order coherences [28]. If the initial droplets are phase coherent, the side peaks are expected to always exhibit the same height, and therefore the corresponding variance should be low. On the other hand, if the initial droplets are not phase coherent, the peak height should fluctuate from realization to realization, and therefore we should observe an increase in the variance of the peak height. Taken together these two effects—fluctuating droplet number and, hence, fringe spacing, as well as incoherent phases between independent droplets—wash out the mean distribution for $a_s = 89a_0$, while the mean distribution for $a_s = 92.5a_0$ shows clear side peaks. This already provides clear evidence for the phase coherence between the droplets in the latter case, with the first side peak [labeled as 1 in Fig. 4(a)] corresponding to nearest-neighbor coherence, and the second peak (labeled as 2) corresponding to next-nearest-neighbor coherence. For atom

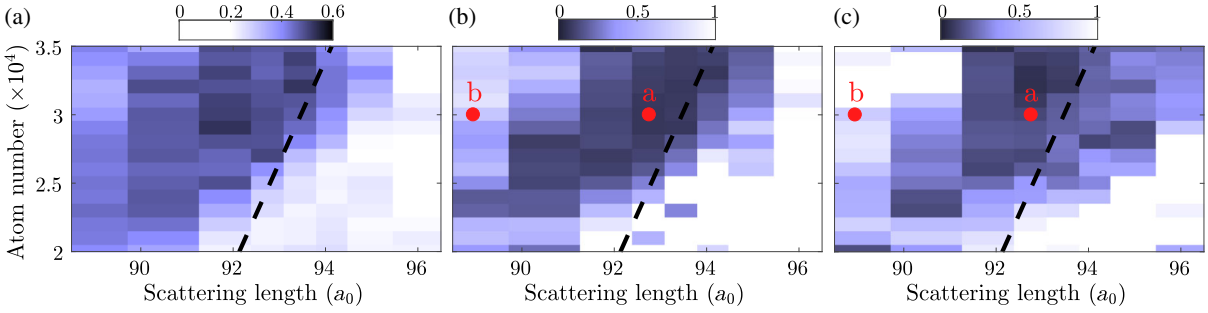

FIG. 5. *In situ* modulation and phase coherence reveal signatures of the theoretical phase diagram. Spectral weight of the observed *in situ* modulation (a), nearest-neighbor coherence (b), and next-nearest-neighbor coherence (c). Only in the range where we observe a density modulation in (a) we also see interference patterns emerging in time of flight (b), (c). For a narrow range of the contact interaction strength, we see clear evidence for phase coherence up to the next-nearest neighbor. The red points labeled "a" and "b" correspond to the exemplary Fourier transforms shown in Figs. 4(a) and (b). The dashed black lines are the same guide to the eye that was shown in Fig. 1(c).

numbers high enough to yield more than three droplets, we can even observe a small signal of next-next-nearest-neighbor interference (labeled as 3).

To quantify the phase coherence we therefore calculate the variance of the height of the Fourier transform side peaks [1 and 2 in Fig. 4(a)] normalized to the peak height [28]. We show these ratios in Figs. 5(b) and 5(c) for different atom numbers and final scattering lengths. The results are in very good agreement with our *in situ* results in Fig. 5(a), as well as the theoretical phase diagram shown in Fig. 1(c). Again we find a sharp phase boundary where the multiple droplet becomes energetically favorable compared to the BEC state. Below this boundary in the respective atom number, we observe no interference and therefore no signal in the Fourier transform. Above this threshold we always see interference; however, only for a small range of contact interactions the coherence between droplets is present. The observed boundaries in all these plots are in agreement with the simulated ground state phase diagram in Fig. 1(c). Combining the *in situ* with the interference results reveals the signatures of the theoretical phase diagram, and we see that for a small range of the contact interaction strength there exists a phase of the system showing both a density modulation as well as phase coherence and therefore the hallmark properties of a supersolid state of matter.

In conclusion, we show theoretically and experimentally that for a narrow range of interaction strengths our dipolar quantum gas of ^{162}Dy atoms exhibits a state that is both density modulated and phase coherent. Together with the dynamical study of the phase coherence in Ref. [25], this observation is the first step towards the realization and identification of a dipolar supersolid, where in contrast to previous works [8–10] the self-organized density modulation is induced by the intrinsic interactions. In order to finally prove the supersolid character of the observed state beyond the phase coherence demonstrated in this work, an experimental proof of phase rigidity, and hence genuine superfluidity, is required. As a next step we therefore plan to investigate the two types of collective excitations, the phonon and phase modes. Another important aspect we plan to study is to extend the lifetime of the observed states, which is currently limited due to three-body losses to approximately 20 ms. This could be accomplished by identifying a region with lower losses in the rich Feshbach spectrum of ^{162}Dy [31,35–37].

We acknowledge insightful discussions with H. P. Büchler, I. Ferrier-Barbut, F. Ferlaino, L. Santos, and A. Pelster. This work is supported by the German Research Foundation (DFG) within FOR2247 under Pf381/16-1, Pf381/20-1, and FUGG INST41/1056-1. T. L. acknowledges support from the EU within Horizon2020 Marie Skłodowska Curie IF (Grant No. 746525 coolDips), as well as support from the Alexander von Humboldt Foundation through a Feodor Lynen Fellowship.

Note added.—Recently, we became aware of another related time-of-flight investigation with Er and Dy atoms [26].

[1] M. Boninsegni and N. V. Prokof'ev, *Colloquium: Supersolids: What and Where Are They?*, Rev. Mod. Phys. **84**, 759 (2012).
[2] A. J. Leggett, *Can a Solid be "Superfluid"?*, Phys. Rev. Lett. **25**, 1543 (1970).
[3] A. F. Andreev and I. M. Lifshitz, *Quatum Theory of Defects in Crystals*, Sov. Phys. JETP **29**, 2 (1969).[JETP **29**, 1107 (1969)].
[4] D. J. Thouless, *The Flow of a Dense Superfluid*, Ann. Phys. (N.Y.) **52**, 403 (1969).
[5] G. V. Chester, *Speculations on Bose-Einstein Condensation and Quantum Crystals*, Phys. Rev. A **2**, 256 (1970).
[6] O. Penrose and L. Onsager, *Bose-Einstein Condensation and Liquid Helium*, Phys. Rev. **104**, 576 (1956).
[7] M. H. W. Chan, R. B. Hallock, and L. Reatto, *Overview on Solid* ^{4}He *and the Issue of Supersolidity*, J. Low Temp. Phys. **172**, 317 (2013).
[8] J. R. Li, J. Lee, W. Huang, S. Burchesky, B. Shteynas, F. Ç. Topi, A. O. Jamison, and W. Ketterle, *A Stripe Phase with Supersolid Properties in Spin-Orbit-Coupled Bose-Einstein Condensates*, Nature (London) **543**, 91 (2017).
[9] J. Léonard, A. Morales, P. Zupancic, T. Esslinger, and T. Donner, *Supersolid Formation in a Quantum Gas Breaking a Continuous Translational Symmetry*, Nature (London) **543**, 87 (2017).
[10] J. Léonard, A. Morales, P. Zupancic, T. Donner, and T. Esslinger, *Monitoring and Manipulating Higgs and Goldstone Modes in a Supersolid Quantum Gas*, Science **358**, 1415 (2017).
[11] M. A. Baranov, M. Dalmonte, G. Pupillo, and P. Zoller, *Condensed Matter Theory of Dipolar Quantum Gases*, Chem. Rev. **112**, 5012 (2012).
[12] Z.-K. Lu, Y. Li, D. S. Petrov, and G. V. Shlyapnikov, *Stable Dilute Supersolid of Two-Dimensional Dipolar Bosons*, Phys. Rev. Lett. **115**, 075303 (2015).
[13] L. Santos, G. V. Shlyapnikov, and M. Lewenstein, *Roton-Maxon Spectrum and Stability of Trapped Dipolar Bose-Einstein Condensates*, Phys. Rev. Lett. **90**, 250403 (2003).
[14] L. Chomaz, R. M. W. Van Bijnen, D. Petter, G. Faraoni, S. Baier, J. H. Becher, M. J. Mark, F. Wächtler, L. Santos, and F. Ferlaino, *Observation of Roton Mode Population in a Dipolar Quantum Gas*, Nat. Phys. **14**, 442 (2018).
[15] D. Petter, G. Natale, R. M. W. van Bijnen, A. Patscheider, M. J. Mark, L. Chomaz, and F. Ferlaino, *Probing the Roton Excitation Spectrum of a Stable Dipolar Bose Gas*, arXiv:1811.12115.
[16] H. Kadau, M. Schmitt, M. Wenzel, C. Wink, T. Maier, I. Ferrier-Barbut, and T. Pfau, *Observing the Rosensweig Instability of a Quantum Ferrofluid*, Nature (London) **530**, 194 (2016).
[17] I. Ferrier-Barbut, H. Kadau, M. Schmitt, M. Wenzel, and T. Pfau, *Observation of Quantum Droplets in a Strongly Dipolar Bose Gas*, Phys. Rev. Lett. **116**, 215301 (2016).
[18] D. S. Petrov, *Quantum Mechanical Stabilization of a Collapsing Bose-Bose Mixture*, Phys. Rev. Lett. **115**, 155302 (2015).

[19] F. Wächtler and L. Santos, *Quantum Filaments in Dipolar Bose-Einstein Condensates*, Phys. Rev. A **93**, 061603(R) (2016).
[20] R. N. Bisset, R. M. Wilson, D. Baillie, and P. B. Blakie, *Ground-State Phase Diagram of a Dipolar Condensate with Quantum Fluctuations*, Phys. Rev. A **94**, 033619 (2016).
[21] L. Chomaz, S. Baier, D. Petter, M. J. Mark, F. Wächtler, L. Santos, and F. Ferlaino, *Quantum-Fluctuation-Driven Crossover from a Dilute Bose-Einstein Condensate to a Macrodroplet in a Dipolar Quantum Fluid*, Phys. Rev. X **6**, 041039 (2016).
[22] I. Ferrier-Barbut, M. Wenzel, M. Schmitt, F. Böttcher, and T. Pfau, *Onset of a Modulational Instability in Trapped Dipolar Bose-Einstein Condensates*, Phys. Rev. A **97**, 011604 (2018).
[23] M. Wenzel, F. Böttcher, T. Langen, I. Ferrier-Barbut, and T. Pfau, *Striped States in a Many-Body System of Tilted Dipoles*, Phys. Rev. A **96**, 053630 (2017).
[24] S. M. Roccuzzo and F. Ancilotto, *Supersolid Behaviour of a Dipolar Bose-Einstein Condensate Confined in a Tube*, arXiv:1810.12229.
[25] L. Tanzi, E. Lucioni, F. Famà, J. Catani, A. Fioretti, C. Gabbanini, and G. Modugno, *Observation of Stable Stripes in a Dipolar Quantum Gas*, arXiv:1811.02613.
[26] L. Chomaz, D. Petter, P. Ilzhöfer, G. Natale, A. Trautmann, C. Politi, G. Durastante, R. M. W. van Bijnen, A. Patscheider, M. Sohmen, M. J. Mark, and F. Ferlaino, *Long-Lived and Transient Supersolid Behaviors in Dipolar Quantum Gases*, arXiv:1903.04375.
[27] I. Ferrier-Barbut, M. Schmitt, M. Wenzel, H. Kadau, and T. Pfau, *Liquid Quantum Droplets of Ultracold Magnetic Atoms*, J. Phys. B **49**, 214004 (2016).
[28] See Supplemental Material at http://link.aps.org/supplemental/10.1103/PhysRevX.9.011051 for further details on the experimental setup, data analysis and numerical simulations.
[29] T. Macrì, F. Maucher, F. Cinti, and T. Pohl, *Elementary Excitations of Ultracold Soft-Core Bosons Across the Superfluid-Supersolid Phase Transition*, Phys. Rev. A **87**, 061602 (2013).
[30] F. Böttcher *et al.* (to be published).
[31] K. Baumann, N. Q. Burdick, M. Lu, and B. L. Lev, *Observation of Low-Field Fano-Feshbach Resonances in Ultracold Gases of Dysprosium*, Phys. Rev. A **89**, 020701(R) (2014).
[32] Because of uncertainty in the measurements of the background scattering length, all experimentally quoted scattering lengths used throughout this work exhibit an uncertainty on the order of 15%. For more information on the determination of the scattering length, see the Supplemental Material [28].
[33] K. B. Davis, M. O. Mewes, M. R. Andrews, N. J. van Druten, D. S. Durfee, D. M. Kurn, and W. Ketterle, *Bose-Einstein Condensation in a Gas of Sodium Atoms*, Phys. Rev. Lett. **75**, 3969 (1995).
[34] Z. Hadzibabic, S. Stock, B. Battelier, V. Bretin, and J. Dalibard, *Interference of an Array of Independent Bose-Einstein Condensates*, Phys. Rev. Lett. **93**, 180403 (2004).
[35] A. Frisch, M. Mark, K. Aikawa, F. Ferlaino, J. L. Bohn, C. Makrides, A. Petrov, and S. Kotochigova, *Quantum Chaos in Ultracold Collisions of Gas-Phase Erbium Atoms*, Nature (London) **507**, 475 (2014).
[36] T. Maier, I. Ferrier-Barbut, H. Kadau, M. Schmitt, M. Wenzel, C. Wink, T. Pfau, K. Jachymski, and P. S. Julienne, *Broad Universal Feshbach Resonances in the Chaotic Spectrum of Dysprosium Atoms*, Phys. Rev. A **92**, 060702(R) (2015).
[37] T. Maier, H. Kadau, M. Schmitt, M. Wenzel, I. Ferrier-Barbut, T. Pfau, A. Frisch, S. Baier, K. Aikawa, L. Chomaz, M. J. Mark, F. Ferlaino, C. Makrides, E. Tiesinga, A. Petrov, and S. Kotochigova, *Emergence of Chaotic Scattering in Ultracold Er and Dy*, Phys. Rev. X **5**, 041029 (2015).

Correction: The inadvertent omission of a marker indicating "Featured in Physics" has been fixed.